Stellar Evolution of High Mass-Loss Stars

Pierre A. Millette

E-mail: pierre.millette@uottawa.ca, Ottawa, Canada

In this paper, we investigate the 37 strongest QSO emission lines of stars of type Q in the catalog of Hewitt & Burbidge [22], as determined by Varshni *et al* [21]. We identify the candidate lines from atomic spectra lines data and determine the estimated T_e range down to the 50% ionic element density for the identified candidate emission lines. This information assists in the classification of Q stars from the 37 QSO dominant emission lines. We use the Hertzsprung-Russell diagram to analyze and determine the role of mass loss in the evolution of stars. We review the nucleosynthesis process that leads from massive O stars to WN and then WC Wolf-Rayet stars as a result of mass loss, and then consider the nucleosynthesis of oxygen in massive stars, showing that ^{16}O oxygen has a significant presence in massive stars beyond the WC stage, until the generation of ^{28}Si, where it disappears. This leads us to postulate more than one population of stars of type Q. One group identified by Varshni [27] with O VI and He II emission lines in their spectra implying much higher temperatures and positioning those QSO stars above the WR region in the HRD. The other group with emission lines dominated by temperatures in the O II and O III range, indicating a lower temperature range of QSO stars with a significant number of ionized oxygen lines and some Si emission lines, in addition to the nitrogen WN and carbon WC lines. We postulate that these QSO spectra correspond to unrecognized Wolf-Rayet stars, in particular WO stars and WSi pre-supernova stars, extending into lower temperatures. In that scenario, Q stars would be the end-state of the Wolf-Rayet evolution process, prior to moving to the supernova state.

1 Introduction

In a recent paper [1], we reviewed the physical process of laser action that is occurring in the stellar atmospheres of stars of type W (Wolf-Rayet) and stars of type Q (QSOs), due to the rapid adiabatic expansion of the stellar atmosphere of these stars, resulting in population inversions in the ionic energy levels due to free electron-ion recombination in the cooling plasma. Laser action in non-LTE stellar atmospheres was first proposed by Menzel in [2] and plasma lasers by Gudzenko in [3]. This results in the extremely strong broad emission lines observed in the spectra of these stars.

Significant work has been performed over the last forty years on the analysis of the emission line spectra of WR stars to understand their classification and evolution [4–15] and is still an ongoing area of research. Previously [1], we noted that a similar effort will be required to understand the classification and evolution of stars of type Q, as has been achieved for Wolf-Rayet stars. In this paper, we take an initial stab at this problem.

In addition, we examine the stellar evolution of high mass-loss stars, characterized by WR and QSO stars, and refine our proposal to enhance the Hertzsprung-Russell Diagram (HRD) by including stars of type W and stars of type Q in the HRD [1]. This allows us to postulate that QSO stars can be identified as unrecognized Wolf-Rayet stars, in particular WO stars and WSi pre-supernova stars, to position them on the HRD, and provide a better understanding of the evolution of high mass-loss stars as displayed in the Hertzsprung-Russell Diagram.

2 Spectra of stars of type W

The emission line spectra of Wolf-Rayet stars are dominated by lines of helium He, carbon C, nitrogen N and oxygen O. The spectra fall into two broad classes: WN stars, which have prominent lines of nitrogen N and helium He ions, with a very strong He II Pickering series ($n = 4 \rightarrow n'$), and essentially no lines of carbon C; and WC stars, where the lines of carbon C and oxygen O are prominent along with the helium He ions, while those of nitrogen N seem to be practically absent [19, p. 485]. An additional subtype WO with strong O VI lines has also recently been added as a separate subtype. The spectra are characterized by the dominance of emission lines, notable for the almost total absence of hydrogen H lines [4].

The number of WR stars in our galaxy is small: the 2001 VII$^{\text{th}}$ catalog of galactic WR stars gave the number at 227 stars, comprised of 127 WN stars, 87 WC stars, 10 WN/WC stars and 3 WO stars [16]. A 2006 update added another 72 WR stars, including 45 WN stars, 26 WC stars and one WO star [17]. The latest number from the August 2020 Galactic Wolf-Rayet Catalogue v1.25 is 667 WR stars [18].

Wolf-Rayet stars have extended atmospheres whose thickness is an appreciable fraction of their stellar radius [19, p. 243]. The material generating the lines is flowing outward from the stellar photosphere. These flows are driven by radiation pressure acting on the stellar atmosphere. Mass loss in stellar winds, particularly in WR stars, is well established [19, pp. 266, 523]. Mass loss rates $\mathcal{M}$ for WR stars are estimated to be of order 10^{-5} up to perhaps 10^{-4} $\mathcal{M}_\odot$/year [20, p. 628] — for comparison, the mass loss rate for the solar

wind is about 10^{-14} $\mathcal{M}_\odot$/year. The massive trans-sonic stellar winds flow velocities in WR stars rise from close to zero in the stellar photosphere to highly supersonic values of order 3 000 km/s within one stellar radius from the surface. Rapid cooling of the strongly ionized plasma results in rapid recombination of the free electrons and the ions into highly excited ionic states, resulting in population inversions and laser action.

3 Spectra of stars of type Q

Similar physical processes are expected to predominate in QSO stars due to the physical similarity of WR and QSO spectra, including the almost total absence of hydrogen H lines. However, while the number of identified WR stars is relatively small, the number of identified QSO stars is larger as we will see later.

Varshni *et al* [21] studied the distribution of QSO spectral emission lines (in the observed frame, i.e. unshifted) of 7 315 QSOs from the catalog of Hewitt & Burbidge [22], of which 5 176 have emission lines. This resulted in a total of 14 277 emission lines in the range λ1271 to λ17993, with the vast majority in the visual range λ3200 to λ5600*.

A number of very strong peaks were found in a histogram of the statistical frequency of the emission lines against wavelength using 4 Å bins. The emission line distribution was expressed in units of standard deviation above a random average, to ensure the lines are statistically significant. The 37 strongest QSO emission lines in the catalog were more than four standard deviations above the random average, of which 13 peaks were above 5σ, of which 3 peaks were above 6σ, of which one peak was above 8σ. These lines are given in Table 1 including the number of standard deviations above a random average.

The 37 QSO emission lines were compared with Wolf-Rayet emission lines in [21], and 27 were found to also occur in WR star spectra, 7 in novae-like star spectra, and two in novae spectra. These are also included in Table 1, along with corresponding candidate element emission lines identification. The lines have been compared against existing sources of data such as Willett's [23] and Bennett's [24] lists of laser transitions observed in laboratories and the *NIST Atomic Spectra Database Lines Data* [25].

In Table 2, we have added the estimated T_e range down to the 50% ionic element density obtained from House [26] for the identified candidate element emission lines. In Tables 3 and 4, we determine the best known line identification and estimated T_e range down to the 50% ionic element density from House [26] respectively, for the 37 QSO emission lines identified in [21]. This provides information to assist in the classification of Q stars from the 37 QSO dominant emission lines.

*The notation λ indicates wavelengths measured in Å.

Varshni [27] also investigated O VI and He II emission lines in the spectra of QSOs, planetary nebulae and Sanduleak stars (WO stars characterized by a strong O VI emission line at λ3811.34 — one example, blue supergiant star Sk -69 202, was identified as the progenitor of supernova 1987A). O VI emission lines imply much higher temperatures (180 000 K < O VI < 230 000 K) than those of Table 4, which are dominated by temperatures in the O II and O III range (16 000 K < O II < 46 000 K and 46 000 K < O III < 73 000 K respectively).

4 Comparative numbers of O, W amd Q stars

The comparative numbers of O, W and Q stars provide hints on their relative classification with respect to their evolution and the Hertzsprung-Russell diagram. O stars are known to be massive hot blue-white stars with surface temperatures in excess of 30 000 K. Wolf-Rayet stars have typical masses in the range of 10–25 $M_\odot$, extending up to 80 $M_\odot$ for hydrogen-rich WN stars [5], and surface temperatures ranging from 30 000 K to around 210 000 K.

Conti *et al* [6] measured the actual numbers and distributions of O stars and Wolf-Rayet stars in a volume-limited sample of stars within 2.5 kpc of the Sun. They found the observed WR/O star number ratio to be given by

$$\frac{\mathrm{WR}}{\mathrm{O}\,(M \geq 40 \pm 5M_\odot)} = 0.36 \pm 0.15\,. \qquad (1)$$

The distribution of WR stars matches that of massive O stars, primarily close to the galactic plane, predominantly in spiral arms Population I stars, which is seen to indicate that WR stars are descendant from the most luminous and massive O stars, likely due to mass loss.

From the latest number of 667 WR stars seen previously in §2, we obtain an estimated number of O stars of

$$1\,850\,^{+1\,350}_{-550}\,,$$

that is between 1 300 and 3 200, from (1). These results are in the same ballpark as available catalogues of O stars, which are still very much a work in progress [28–33]. This number is similar to that of planetary nebulae with about 2 700 known in 2008 (MASH catalogue) [34, 35]. These distributions and numbers of O stars and Wolf-Rayet stars agree with the changes to the Hertzsprung-Russell diagram suggested in [1] to include more massive and hotter stars of type W beyond the stars of type O B.

For the number of stars of type Q, we saw previously in §3 that the Hewitt & Burbidge catalog of 1993 [22] included 7 315 QSOs, of which 5 176 have emission lines, which represents 11 times the current number of known WR stars. However, the latest edition of the *Sloan Digital Sky Survey Quasar Catalog DR16Q* [36] to August 2018, includes a total of 750 414 quasars (100 times the 1993 Hewitt & Burbidge catalog number). This represents 1 125 times the number of WR

QSO λ (Å)	σ	WR λ (Å)	NL λ (Å)	Nova λ (Å)	Emitter λ candidates	Emitter λ candidates	Emitter λ candidates
3356	4.0	3358.6			N III λ3355	O III λ3355.9	C III λ3358
3489	4.1	3493			O IV λ3489.83	O II λ3488.258	O II λ3494.04
3526	6.7				C V λ3526.665	O II λ3525.567	
3549	4.3				O II λ3549.091	Si III λ3549.42	
3610	4.6	⟨3609.5⟩			C III λ3609.6	He I λ3613.6	N II λ3609.097
3648	5.4	3645.4			O II λ3646.56	O IV λ3647.53	O IV λ3642
3683	4.4	3687	3685.10		O II λ3683.326	O III λ3682.383/6.393	N IV λ3689.94
3719	4.7	⟨3721.0⟩			O III λ3721	O V λ3717.31	
3770	4.7	⟨3769.5⟩			N III λ3770.36/1.05	Si III λ3770.585	O III λ3774.026
3781	5.3	3784.8			He II λ3781.68	O II λ3784.98	N III λ3779
3831	5.1	3829.9			He II λ3833.80	C II λ3831.726	O II λ3830.29
3842	4.7				O IV λ3841.07	N II λ3842.187/.449	O II λ3842.815
3855	5.0	3856.6			N II λ3855.096/.374	O II λ3856.134	He II λ3858.07
3890	8.4	⟨3889.0⟩			He I λ3888.64	C III λ3889.18/.670	O III λ3891.759
3903	5.6		3903.0		O III λ3903.044		
3952	4.4	⟨3954.2⟩			O II λ3954.3619	Si III λ3952.23/3.071	
4012	6.0	⟨4008.4⟩			N III λ4007.88	N III λ4013.00	Si III λ4010.236
4135	4.8	?			N III λ4134.91/6.07	O V λ4134.11	N II λ4133.673
4276	5.9	?	4276.6	4275.5	O II λ4275.5	O II λ4275.994	O II λ4276.620
4524	4.7	⟨4520.4⟩			N III λ4523.56/7.9	O III λ4524.2/7.3	O V λ4522.66
4647	4.0	4650.8			C III λ4647.40/51.35	O II λ4647.803/9.1348	O III λ4649.973
4693	4.7	?	4697.0		O II λ4693.195	N II λ4694.274/7.638	O III λ4696.225
4771	4.1	?	4772.1		N IV λ4769.86	O IV λ4772.6	O II λ4773.782
4801	4.3	⟨4799.6⟩			O IV λ4800.74	Si III λ4800.43	
4817	4.4	4814.6	4814.4		O IV λ4813.15	Si III λ4813.33/9.72	N II λ4815.617
4910	4.9	4909.2			N III λ4904.78	Si III λ4912.310	
4925	4.5	⟨4924.6⟩			O II λ4924.531	He I λ4921.9	
4956	7.0	4958		4959.0	O II λ4955.705	O III λ4958.911	
5018	5.6	⟨5018.3⟩			He I λ5015.67	C IV λ5015.9/7.7	N II λ5016.39
5035	4.2				N III λ5038.31		
5049	5.5	5049.9			He I λ5047.7	C III λ5048.95	O III λ5049.870
5096	5.5	5092.9			N III λ5097.24	O III λ5091.880	O II λ5090.920
5111	4.8		5111.5		O II λ5110.300/1.913	Si III λ5111.1	O III λ5112.18
5173	4.6	5171.1			N II λ5171.266/2.344	N II λ5173.385	O III λ5171.29
5266	5.3	5266.3			O III λ5268.301		
5345	4.1	5343.3			O II λ5344.104	C III λ5345.881	
5466	4.0	⟨5469.9⟩			Si II λ5466.43/9.21	O V λ5471.12	Si III λ5473.05

Table 1: QSO emission lines in the range λ3200 to λ5600 from Varshni *et al* [21] (NL: novae-like star).

QSO λ (Å)	σ	WR λ (Å)	NL λ (Å)	Nova λ (Å)	Emitter T_e (K) candidates	Emitter T_e (K) candidates	Emitter T_e (K) candidates
3356	4.0	3358.6			33k < N III < 65k	46k < O III < 73k	29k < C III < 58k
3489	4.1	3493			73k < O IV < 130k	16k < O II < 46k	16k < O II < 46k
3526	6.7				92k < C V < 730k	16k < O II < 46k	
3549	4.3				16k < O II < 46k	18k < Si III < 46k	
3610	4.6	⟨3609.5⟩			29k < C III < 58k	He I < 26k	18k < N II < 33k
3648	5.4	3645.4			16k < O II < 46k	73k < O IV < 130k	73k < O IV < 130k
3683	4.4	3687	3685.10		16k < O II < 46k	46k < O III < 73k	65k < N IV < 103k
3719	4.7	⟨3721.0⟩			46k < O III < 73k	146k < O V < 184k	
3770	4.7	⟨3769.5⟩			33k < N III < 65k	18k < Si III < 46k	46k < O III < 73k
3781	5.3	3784.8			26k < He II < 73k	16k < O II < 46k	33k < N III < 65k
3831	5.1	3829.9			26k < He II < 73k	15k < C II < 29k	16k < O II < 46k
3842	4.7				73k < O IV < 130k	18k < N II < 33k	16k < O II < 46k
3855	5.0	3856.6			18k < N II < 33k	16k < O II < 46k	26k < He II < 73k
3890	8.4	⟨3889.0⟩			He I < 26k	29k < C III < 58k	46k < O III < 73k
3903	5.6		3903.0		46k < O III < 73k		
3952	4.4	⟨3954.2⟩			16k < O II < 46k	18k < Si III < 46k	
4012	6.0	⟨4008.4⟩			33k < N III < 65k	18k < Si III < 46k	
4135	4.8	?			33k < N III < 65k	146k < O V < 184k	18k < N II < 33k
4276	5.9	?	4276.6	4275.5	16k < O II < 46k		
4524	4.7	⟨4520.4⟩			33k < N III < 65k	46k < O III < 73k	146k < O V < 184k
4647	4.0	4650.8			29k < C III < 58k	16k < O II < 46k	46k < O III < 73k
4693	4.7	?	4697.0		16k < O II < 46k	18k < N II < 33k	46k < O III < 73k
4771	4.1	?	4772.1		65k < N IV < 103k	73k < O IV < 130k	16k < O II < 46k
4801	4.3	⟨4799.6⟩			73k < O IV < 130k	18k < Si III < 46k	
4817	4.4	4814.6	4814.4		73k < O IV < 130k	18k < Si III < 46k	18k < N II < 33k
4910	4.9	4909.2			33k < N III < 65k	18k < Si III < 46k	
4925	4.5	⟨4924.6⟩			16k < O II < 46k	He I < 26k	
4956	7.0	4958		4959.0	16k < O II < 46k	46k < O III < 73k	
5018	5.6	⟨5018.3⟩			He I < 26k	65k < C IV < 92k	18k < N II < 33k
5035	4.2				33k < N III < 65k		
5049	5.5	5049.9			He I < 26k	29k < C III < 58k	46k < O III < 73k
5096	5.5	5092.9			33k < N III < 65k	46k < O III < 73k	16k < O II < 46k
5111	4.8		5111.5		16k < O II < 46k	18k < Si III < 46k	46k < O III < 73k
5173	4.6	5171.1			18k < N II < 33k	46k < O III < 73k	
5266	5.3	5266.3			46k < O III < 73k		
5345	4.1	5343.3			16k < O II < 46k	29k < C III < 58k	
5466	4.0	⟨5469.9⟩			8.2k < Si II < 18k	146k < O V < 184k	18k < Si III < 46k

Table 2: QSO emission lines in the range λ3200 to λ5600 with estimated T_e range down to the 50% ionic element density from House [26].

QSO λ (Å)	WR λ (Å)	NL λ (Å)	Nova λ (Å)	Emitter QSO λ	Emitter WR λ	Emitter NL λ	Emitter Nova λ
3356	3358.6			O III λ3355.9	C III λ3358		
3489	3493			O II λ3488.258	O II λ3494.04		
3526				O II λ3525.567			
3549				O II λ3549.091			
3610	⟨3609.5⟩			C III λ3609.6			
3648	3645.4			O IV λ3647.53	O II λ3646.56		
3683	3687	3685.10		O II λ3683.326	O III λ3686.393	O III λ3686.393	
3719	⟨3721.0⟩			O III λ3721	O III λ3721		
3770	⟨3769.5⟩			N III λ3770.36	N III λ3770.36		
3781	3784.8			He II λ3781.68	O II λ3784.98		
3831	3829.9			C II λ3831.726	O II λ3830.29		
3842				N II λ3842.187			
3855	3856.6			N II λ3855.096	O II λ3856.134		
3890	⟨3889.0⟩			C III λ3889.670	C III λ3889.18		
3903		3903.0		O III λ3903.044		O III λ3903.044	
3952	⟨3954.2⟩			Si III λ3952.23	O II λ3954.3619		
4012	⟨4008.4⟩			N III λ4013.00	N III λ4007.88		
4135	?			N III λ4134.91			
4276	?	4276.6	4275.5	O II λ4275.994		O II λ4276.620	O II λ4275.5
4524	⟨4520.4⟩			O III λ4524.2	O V λ4522.66		
4647	4650.8			C III λ4647.40	C III λ4651.35		
4693	?	4697.0		O II λ4693.195		O III λ4696.225	
4771	?	4772.1		N IV λ4769.86		O IV λ4772.6	
4801	⟨4799.6⟩			O IV λ4800.74	O IV λ4800.74		
4817	4814.6	4814.4		N II λ4815.617	Si III λ4813.33	O IV λ4813.15	
4910	4909.2			Si III λ4912.310	Si III λ4912.310		
4925	⟨4924.6⟩			O II λ4924.531	O II λ4924.531		
4956	4958		4959.0	O II λ4955.705	O III λ4958.911		O III λ4958.911
5018	⟨5018.3⟩			C IV λ5017.7	C IV λ5017.7		
5035				N III λ5038.31?			
5049	5049.9			C III λ5048.95	O III λ5049.870		
5096	5092.9			N III λ5097.24	O III λ5091.880		
5111		5111.5		Si III λ5111.1		O II λ5111.913	
5173	5171.1			N II λ5173.385	N II λ5171.266		
5266	5266.3			O III λ5268.301?	O III λ5268.301?		
5345	5343.3			O II λ5344.104	O II λ5344.104		
5466	⟨5469.9⟩			Si II λ5466.43	Si II λ5469.21		

Table 3: QSO emission lines in the range λ3200 to λ5600 with best known line identification.

QSO λ (Å)	WR λ (Å)	NL λ (Å)	Nova λ (Å)	Emitter QSO T_e	Emitter WR T_e	Emitter NL T_e	Emitter Nova T_e
3356	3358.6			46k<O III<73k	29k<C III<58k		
3489	3493			16k<O II<46k	16k<O II<46k		
3526				16k<O II<46k			
3549				16k<O II<46k			
3610	⟨3609.5⟩			29k<C III<58k			
3648	3645.4			73k<O IV<130k	16k<O II<46k		
3683	3687	3685.10		16k<O II<46k	46k<O III<73k	46k<O III<73k	
3719	⟨3721.0⟩			46k<O III<73k	46k<O III<73k		
3770	⟨3769.5⟩			33k<N III<65k	33k<N III<65k		
3781	3784.8			26k<He II<73k	16k<O II<46k		
3831	3829.9			15k<C II<29k	16k<O II<46k		
3842				18k<N II<33k			
3855	3856.6			18k<N II<33k	16k<O II<46k		
3890	⟨3889.0⟩			29k<C III<58k	29k<C III<58k		
3903		3903.0		46k<O III<73k		46k<O III<73k	
3952	⟨3954.2⟩			18k<Si III<46k	16k<O II<46k		
4012	⟨4008.4⟩			33k<N III<65k	33k<N III<65k		
4135	?			33k<N III<65k			
4276	?	4276.6	4275.5	16k<O II<46k		16k<O II<46k	16k<O II<46k
4524	⟨4520.4⟩			46k<O III<73k	146k<O V<184k		
4647	4650.8			29k<C III<58k	29k<C III<58k		
4693	?	4697.0		16k<O II<46k		46k<O III<73k	
4771	?	4772.1		65k<N IV<103k		73k<O IV<130k	
4801	⟨4799.6⟩			73k<O IV<130k	73k<O IV<130k		
4817	4814.6	4814.4		18k<N II<33k	18k<Si III<46k	73k<O IV<130k	
4910	4909.2			18k<Si III<46k	18k<Si III<46k		
4925	⟨4924.6⟩			16k<O II<46k	16k<O II<46k		
4956	4958		4959.0	16k<O II<46k	46k<O III<73k		46k<O III<73k
5018	⟨5018.3⟩			65k<C IV<92k	65k<C IV<92k		
5035				33k<N III<65k			
5049	5049.9			29k<C III<58k	46k<O III<73k		
5096	5092.9			33k<N III<65k	46k<O III<73k		
5111		5111.5		18k<Si III<46k		16k<O II<46k	
5173	5171.1			18k<N II<33k	18k<N II<33k		
5266	5266.3			46k<O III<73k	46k<O III<73k		
5345	5343.3			16k<O II<46k	16k<O II<46k		
5466	⟨5469.9⟩			8.2k<Si II<18k	8.2k<Si II<18k		

Table 4: QSO emission lines in the range λ3200 to λ5600 with best known line identification and with estimated T_e range down to the 50% ionic element density from House [26].

stars — quite obviously, we are dealing with a phenomenon that is not as rare as O stars, WR stars or planetary nebulae.

There is a total of between 100 billion and 400 billion stars estimated in the Milky Way galaxy. The number of QSOs just represents about 2×10^{-6} times the estimated number of stars in the Milky Way galaxy, thus a fairly rare phenomenon, even if it is about 10^3 times more numerous than Wolf-Rayet stars. This requires further analysis in terms of understanding and positioning stars of type Q on the Hertzsprung-Russell diagram, with some of the QSOs with strong O VI lines [27] likely lying beyond the stars of type W O B as suggested in [1] and some having temperatures in the WR star range. The estimated number of quasars may be inflated due to the tendency in modern astronomy to identify redshifts as a predominant causative factor, but even if it is off by a factor of ten, the QSO phenomenon is much more common than Wolf-Rayet stars, in spite of their similarity.

We take a brief look at novae and novae-like stars [37], given their presence in Tables 1 to 4. These are part of what are known as *cataclysmic variables* (CVs), which are binary star systems consisting of a white dwarf and a normal star companion. Matter transfer to the white dwarf from the companion star results in the formation of an accretion disk around the white dwarf, which produces occasional cataclysmic outbursts of matter.

A main sequence star in a binary system evolves into a white dwarf for a mass below the Chandrasekhar limit (white dwarf maximum mass limit of about $1.4\,M_\odot$). Novae are CV white dwarfs that undergo an eruption that can change by 10–12 magnitudes in a few hours. They are subdivided into classical novae (single observed eruption with a spectroscopically detected shell of ejected matter), recurrent novae (multiple observed outbursts with detected shell of matter), and dwarf nova (multiple observed eruptions with no shell of detected matter).

Nova-like (NL) variables include all "non-eruptive" cataclysmic variables. These systems have spectra, mostly emission spectra, indicating that they are possibly novae that have not been observed. A catalogue of cataclysmic variables to 2006 contains 1 600 CVs [38].

5 The Hertzsprung-Russell diagram and the role of mass loss in the evolution of stars

The Hertzsprung-Russell diagram is a powerful tool to analyze and represent stellar evolution and understand the characteristics and properties of stars. Most HR diagrams cover the temperature range 40 000 K and below, thus ignoring hotter and more massive stars of interest in this work.

From an idealized perspective, the main sequence is a vaguely diagonal curve running from the upper left to the lower central part of the diagram; from it, vaguely horizontal branches tend to the right of the diagram. The main sequence is known as the Zero-Age Main Sequence (ZAMS) which a star enters when it starts core hydrogen burning; massive stars (O,B) rapidly burn the hydrogen in $\sim3\times10^6$ years, while low mass stars (M) burn the hydrogen more slowly in $\sim2\times10^{11}$ years.

As the core hydrogen becomes depleted, the star moves towards the horizontal portion of the diagram, and once core hydrogen burning terminates, it moves towards the right on the horizontal branch, becoming a red giant for cooler less massive stars (G) or a red supergiant for hot massive stars (O). Interestingly enough, in a recent study of stars of types O and early-B in the Wing of the Small Magellanic Cloud (SMC) satellite galaxy, Ramachandra *et al* [39] have found that the above scenario applies to O stars with initial mass below $\sim30\,M_\odot$, while O stars with initial mass above $\sim30\,M_\odot$ appear to always stay hot.

Once a star has exhausted its core hydrogen (and hydrogen shell), it enters its core helium burning phase. In Fig. 1, we reproduce the very important Hertzsprung-Russell diagram of [39] for the stars of types O and early-B of the SMC Wing: it covers the temperature range up to 200 000 K, shows the Helium Zero-Age Main Sequence (He-ZAMS) and also exceptionally includes the Wolf-Rayet (WR) stars. As we saw previously, the red giant and supergiant scenario, where the hydrogen-depleted stars veer off the ZAMS to the right, applies to O stars with initial mass below $\sim30\,M_\odot$ (shaded portion in Fig. 1). However, as we see in Fig. 1, for O stars with initial mass above $\sim30\,M_\odot$, the hydrogen-depleted stars veer off the ZAMS to the left to become WR stars, which are known to be hydrogen-deficient. Of the main factors affecting massive star evolution, focusing on rotation, binarity and mass-loss rate, we believe this dichotomy in behaviour is because of the massive mass loss in WR stars as seen in §2 driving laser action in their stellar atmospheres, while [39] believes it is due to the rapid rotation of the stars, leading to efficient mixing of the stellar interior and quasi-chemically homogeneous evolution (QCHE) .

The work of Ramachandra *et al* [39] is an excellent example of using one of the better tools at our disposal to understand stellar astrophysical problems by performing analysis on the observed data in neighbouring galaxies, as mentioned in [1]. Along those lines, Hainich *et al* [40] has performed an analysis of single WN Wolf-Rayet stars in the Small Magellanic Cloud. Fig. 2 is a reproduction of the Hertzsprung-Russell diagram for the WN stars of the Small Magellanic Cloud (SMC) from Hainich *et al* [40], which also includes the WN stars of the Large Magellanic Cloud (LMC) and the Milky Way (MW). It corresponds to the upper left portion of Ramachandra's HRD for log luminosity > 5.2 and temperatures > 25 000 K (in the WR region), and provides details for the WNE and WNL populations of the SMC, LMC and Milky Way galaxy. WNE is a subtype for early-type WN stars (WN2–WN5), while WNL is for late-type WN stars (WN6–WN11).

This HRD provides more details on WN star properties:

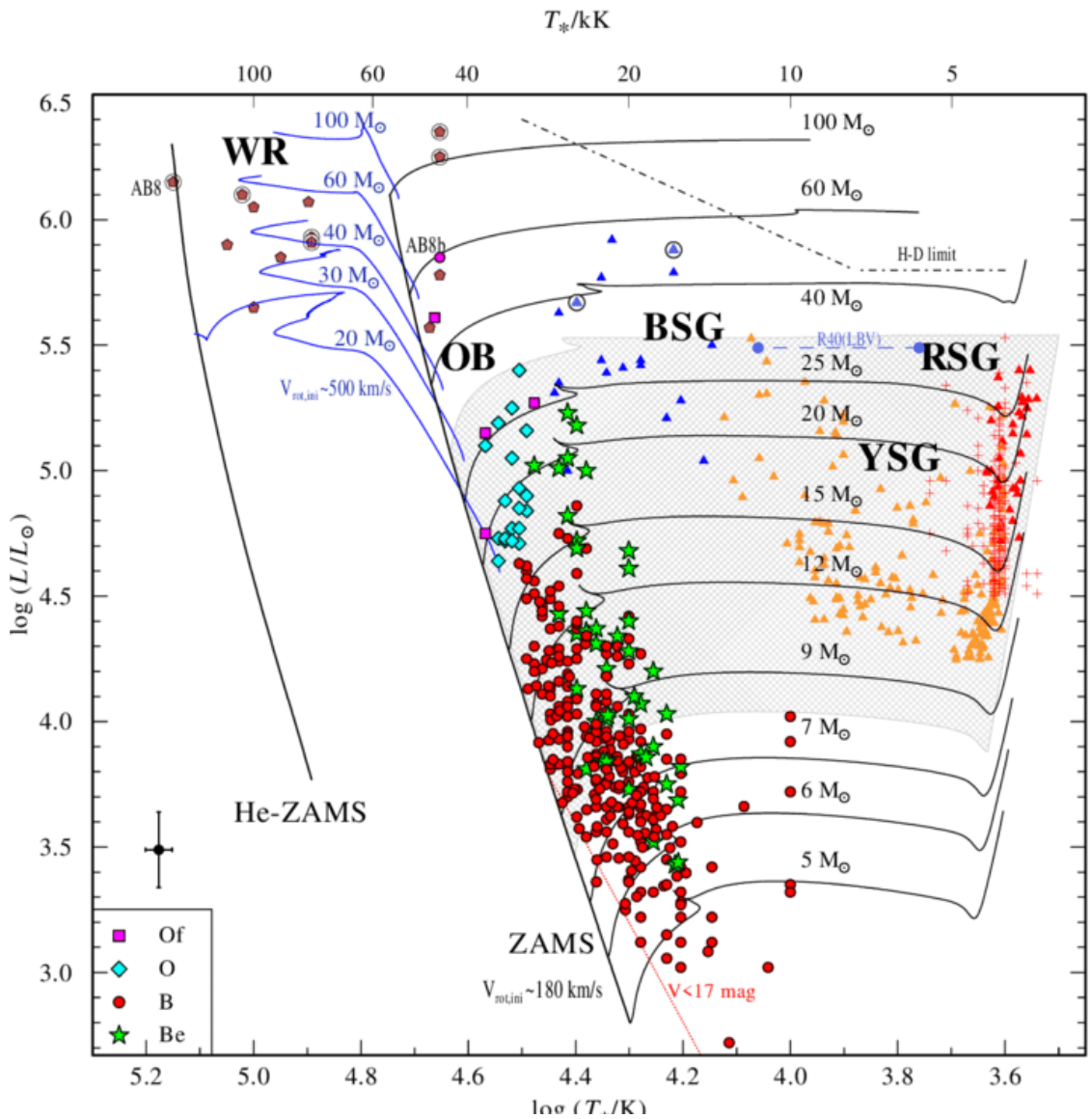

Fig. 1: Hertzsprung Russell diagram for massive stars in the Wing of the SMC reproduced from Ramachandra *et al* [39]. Typical error bar shown at bottom left corner. The brown pentagons represent WR stars (encircled if in a binary system), yellow symbols represent yellow supergiant (YSG) stars, blue triangles for BSGs (blue supergiant), and red triangles for RSGs (red supergiant). Black tracks show standard stellar evolutionary paths, while the blue tracks show the paths of quasi-chemically homogeneously evolving (QCHE) WR stars.

most WNE stars are on the left of the ZAMS line, but to the right of the He-ZAMS line; while most WNL stars are on the right of the ZAMS line, but close to it in the hydrogen depletion region of the stellar evolution curve, above log luminosity > 5.5 corresponding to stellar masses where the stars do not evolve into colder supergiants, as mentioned by Ramachandra *et al* [39]. See also Figures 7 and 8 of [11] for WN stars in the Large Magellanic Cloud. Thus, the calculated WR star evolution curves that extend to the right into lower temperature supergiant stars, usually seen in published HR diagrams, are likely incorrect, especially considering their high mass-loss rates driving laser action in their stellar atmospheres. The Luminous Blue Variable (LBV) stars included in such stellar evolution curves are more than likely variable Wolf-Rayet stars.

Metallicity is a measure of the abundance of elements heavier than hydrogen or helium in an astronomical object. Hence stars and nebulae with relatively high carbon, nitrogen, oxygen, neon, *etc* abundance have high metallicity values z (the metallicity of the Sun is $z = 0.0134$). The degree of wind mass-loss of WR stars depends on their initial metallicity. Metallicity thus has an effect on the evolution of massive stars and of WR stars in particular. The Small Magellanic Cloud is a low-metallicity environment, lower than the metal-

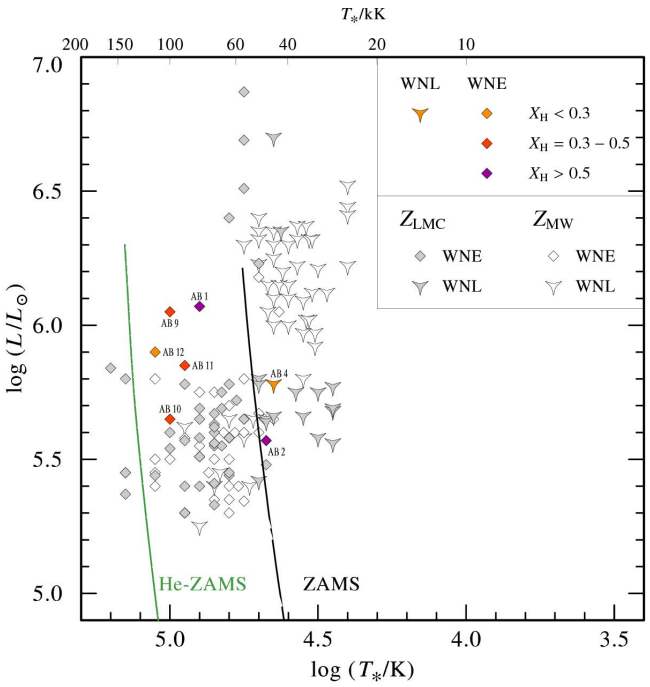

Fig. 2: Hertzsprung-Russell diagram for WN stars in the Small Magellanic Cloud (SMC) reproduced from Hainich *et al* [40]. Includes the Large Magellanic Cloud (LMC gray-filled symbols) and Milky Way (MW open symbols) WN stars.

deficient Large Magellanic Cloud itself lower in comparison to the Milky Way. SMC WN stars thus have on average lower mass-loss rates and weaker winds than their counterparts in the LMC and the Milky Way [40]. A reduction in the mass-loss rate at lower metallicity results in weaker emission line spectra in WR stars, a clear indication that the strong emission lines are due to the mass-loss rate which results in lasing transitions as seen in [1].

The process that leads from massive O stars to WR stars as a result of mass loss is believed to be well understood [41]. As a massive star evolves and loses mass, it eventually exposes He and N (the products of CNO burning) at the surface and is then spectroscopically identified as a WN star. As the star continues losing mass, it eventually exposes C and O (the products of He burning) at the surface and is then identified as a WC star. The mass loss rates depend on the metallicity of the environment which results in different WC/WN ratios as observed in Local Group galaxies. This is reflected in lower WC/WN ratios in lower metallicity environments: $(WC/WN)_{SMC} = 0$, $(WC/WN)_{LMC} = 0.25$ and $(WC/WN)_{MW} = 1$ [40].

Meyer *et al* [42] have analyzed the nucleosynthesis of oxygen in massive stars (see also [43]). In their model calculations, they find that in the WC stars, the oxygen in the C/O zone is dominated by the ^{16}O isotope. This matter which is part of the helium burning core, does not partake in the carbon shell burning. This is followed by the O/Ne zone where the star experiences convective shell carbon burning and where there is a slight ^{16}O depletion, but where ^{16}O still strongly dominates the oxygen abundances. This is followed by the O/Si zone where the star experiences shell neon burning which increases the ^{16}O slightly. Finally, the star burns its ^{16}O into ^{28}Si and heavier isotopes both in pre-supernova and supernova nucleosynthesis, devoid of any oxygen.

Thus they find that oxygen has a significant presence in massive stars beyond the WC stage, until the generation of ^{28}Si, where it disappears. Considering Table 3, this behavior is interesting due to the presence of, in addition to the ionized nitrogen and carbon lines, a significant number of ionized oxygen lines, and the presence of some standalone silicon lines.

6 The evolution of stars of type Q

Given all of these considerations, how does the evolution of stars of type Q fit in the Hertzsprung-Russell diagram? We know that they are undergoing high mass-loss due to the broad high intensity spectral lines indicative of laser action in their stellar atmosphere. As seen in Table 3, their emission spectra are dominated by lines of ionized He, C, N, O and Si, with many lines in common with WR stars and novae-like stars.

There may be more than one population of stars of type Q. One group identified by Varshni [27] with O VI and He II emission lines in their spectra, in common with planetary nebulae and Sanduleak stars, implies much higher temperatures in the range 180 000 K < O VI < 230 000 K, positioning those QSO stars above the WR region in the HRD of Ramachandra *et al* [39] given in Fig. 1. However, there are emission lines as given in Table 3, which are dominated by temperatures in the O II and O III range (16 000 K < O II < 46 000 K and 46 000 K < O III < 73 000 K respectively), indicating a lower temperature range of QSO stars.

Indeed, as seen previously, these QSO emission line spectra have a significant number of ionized oxygen lines. WN and WC Wolf-Rayet stars predominate, with WN stars having the upper hand in low metallicity environments. However, the recently recognized WO lines are rare — could the QSO spectra with a significant number of ionized O emission lines and some Si emission lines, correspond to unrecognized much more numerous WO Wolf-Rayet stars extending into lower temperatures? They would in effect fill up the Hertzsprung-Russell diagram of Ramachandra *et al* [39] given in Fig. 1 in the range 16 000 K < T_e < 73 000 K for stellar masses above ~30 $M_\odot$.

For example, if we look at QSO 3C 273, the first radio source quasar for which an optical counterpart was identified in 1963, its spectrum consisted of one strong emission line and one medium to weak strength line (λ5637, λ7588). Comparing these lines against existing sources of data [23–25], the following identifications are obtained from the *NIST*

Atomic Spectra Database Lines Data and the corresponding estimated T_e range down to the 50% ionic element density obtained from House [26] for the identified candidate element emission lines (see Table 5). Based on this information, we would be inclined to conclude that the broad observed emission lines correspond to C II λ5640.55 and O II λ7593, with an estimated stellar temperature in the range 16 000 K < T_e < 29 000 K.

QSO λ (Å)	strength	Emitter λ	Emitter T_e
5637	S	C II λ5640.55	15k<C II<29k
		Si II λ5633/41	8.2k<Si II<18k
7588	M-W	O II λ7593	16k<O II<46k
		C III λ7586.41	29k<C III<58k
		O IV λ7585.74	73k<O IV<130k

Table 5: QSO 3C 273 observed emission lines, identification and estimated T_e range down to the 50% ionic element density obtained from House [26].

7 Laser action in WR and QSO stars

The details of the process of laser action in the stellar atmospheres of Wolf-Rayet stars and Quasi-Stellar Object stars are given in [1]. The physical process of population inversions in expanding stellar atmospheres led Varshni to formulate his Plasma Laser Star (PLS) model as an explanation of the spectra of Wolf-Rayet stars and Quasi-Stellar Objects [47–52]. Model calculations starting from an initial element number density of 10^{14} cm^{-3} are performed for a grid of free electron number density n_e and temperature T_e values. The population inversion is displayed on $n_e - T_e$ diagrams showing contours of equal P or α', where [44]

$$P = \frac{n_q}{\omega_q} - \frac{n_p}{\omega_p}, \tag{2}$$

where n_q is the population density and ω_q is the statistical weight of level q, and [45, p, 23]

$$\alpha = \sqrt{\frac{\ln 2}{\pi}} \left(\frac{\omega_q A_{q\to p}}{4\pi}\right) \frac{P\lambda_0^2}{\Delta\nu}, \tag{3}$$

where λ_0 is the centre wavelength of the transition, $\Delta\nu$ is the linewidth, $A_{q\to p}$ is the Einstein probability coefficient for spontaneous transition from level q to p, and $\alpha' = \alpha\,\Delta\nu$. Fig. 3 shows a typical $n_e - T_e$ diagram with equi-α' contours for inversely populated transition $6f \to 5d$ of C IV.

Taking Quasi-Stellar Objects to be local stellar objects instead of distant galactic objects eliminates the problems associated with their currently accepted cosmological interpretation: energy source, superluminal velocities, optical variability, quasar proper motions [53, 54], quasar binary systems [55, 56], naked (no nebulosity) quasars, *etc*. The properties of QSOs are similar to those of WR stars and, as stars, those are easily explainable in terms of commonly known physical processes. QSO stars could very well be unrecognized Wolf-Rayet stars, in particular WO stars and WSi pre-supernova stars. In that case, Q stars would be the end-state of the Wolf-Rayet evolution process and would account for their number larger than WN and WC W stars (about 10^3 times), prior to moving to the supernova state.

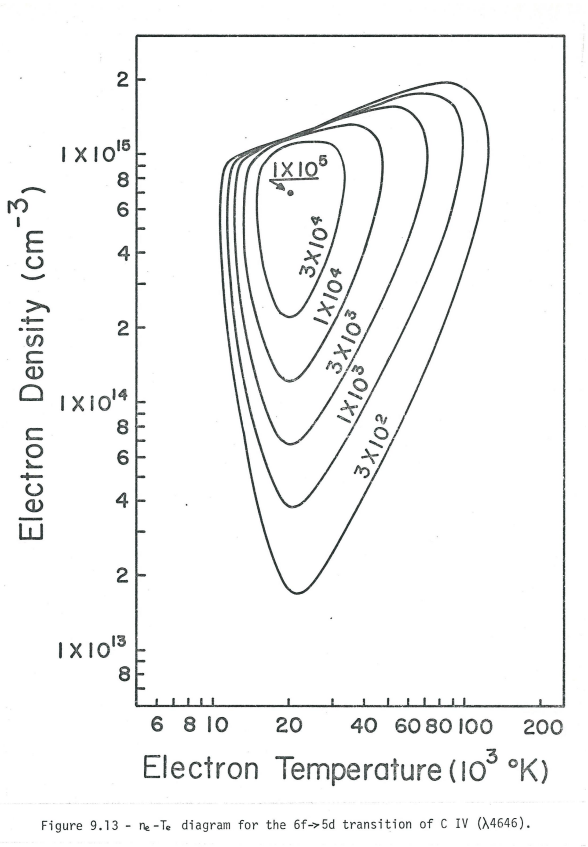

Fig. 3: Typical $n_e - T_e$ diagram showing laser gain equi-α' contours in cm^{-1} s^{-1} for the $6f \to 5d$ transition of C IV [46, p. 257].

8 Discussion and conclusion

In this paper, we have investigated the 37 strongest QSO emission lines of stars of type Q in the catalog of Hewitt & Burbidge [22], investigated by Varshni *et al* [21]. We have used Willett's [23] and Bennett's [24] lists of laser transitions observed in laboratories and the *NIST Atomic Spectra Database Lines Data* [25] to identify candidate lines. In addition, we have determined the estimated T_e range down to the 50% ionic element density obtained from House [26] for the identified candidate element emission lines. This information assists in the classification of Q stars from the 37 QSO dominant

emission lines.

We have summarized the comparative numbers of O, W, and Q stars, novae and planetary nebulae to provide hints on their relative classification with respect to their evolution and the Hertzsprung-Russell diagram. The Hertzsprung-Russell diagram is a powerful tool to analyze and represent stellar evolution and has been used to determine the role of mass loss in the evolution of stars. In particular, we have considered the very important HR diagram of Ramachandra *et al* [39] for the stars of types O and early-B of the SMC Wing as it covers the temperature range up to 200 000 K, shows the Helium Zero-Age Main Sequence (He-ZAMS) and also exceptionally includes the Wolf-Rayet (WR) stars. In addition, their determination that hydrogen-depleted O stars with initial mass below $\sim 30\, M_{\odot}$ evolve off the ZAMS to the right into colder red giants and supergiants, while hydrogen-depleted O stars with initial mass above $\sim 30\, M_{\odot}$ appear to always stay hot and veer off the ZAMS to the left to become Wolf-Rayet stars, beyond the O stars, is indicative of laser action in their stellar atmosphere.

We have reviewed the nucleosynthesis process that leads from massive O stars to WN and then WC Wolf-Rayet stars as a result of mass loss. We then considered the nucleosynthesis of oxygen in massive stars and found that ^{16}O oxygen has a significant presence in massive stars beyond the WC stage, until the generation of ^{28}Si, where it disappears. This has lead us to postulate more than one population of stars of type Q. One group identified by Varshni [27] with O VI and He II emission lines in their spectra implying much higher temperatures and positioning those QSO stars above the WR region in the HRD of Ramachandra *et al* [39].

The other group with emission lines dominated by temperatures in the O II and O III range, indicating a lower temperature range of QSO stars with a significant number of ionized oxygen lines, in addition to the nitrogen WN and carbon WC lines. We postulate that these QSO spectra, with a significant number of ionized O emission lines and some Si emission lines, correspond to unrecognized Wolf-Rayet stars, in particular WO stars and WSi pre-supernova stars, extending into lower temperatures. They in effect fill up the HRD of Ramachandra *et al* [39] in the range $16\,000\,\mathrm{K} < T_e < 73\,000\,\mathrm{K}$ for stellar masses above $\sim 30\, M_{\odot}$. In that scenario, Q stars would be the end-state of the Wolf-Rayet evolution process and would account for their number larger than WN and WC W stars, prior to moving to the supernova state.

Received on February 15, 2021

References

1. Millette P. A. Laser Action in the Stellar Atmospheres of Wolf-Rayet Stars and Quasi-Stellar Objects (QSOs). *Prog. Phys.*, 2021, v. 17 (1), 71–82.
2. Menzel D. H. Laser Action in non-LTE Atmospheres. International Astronomical Union Colloquium, Volume 2: Spectrum Formation in Stars With Steady-State Extended Atmospheres, 1970, 134–137.
3. Gudzenko L. L., Shelepin L. A., Yakovlenko S. I. Amplification in recombining plasmas (plasma lasers). *Usp. Fiz. Nauk*, 1974, v. 114, 457. *Sov. Phys. - Usp.*, 1975, v. 17, 848.
4. Abbott D. C. and Conti P. S. Wolf-Rayet Stars. *Ann. Rev. Astron. Astrophys.*, 1987, v. 25, 113–150.
5. Crowther P. A. Physical Properties of Wolf-Rayet Stars. *Annu. Rev. Astron. Astrophys.*, 2007, v. 45, 177–219. arXiv: astro-ph/0610356v2.
6. Conti P. S. and Garmany C. D., De Loore C. and Vanbeveren D. The Evolution of Massive Stars: The Numbers and Distribution of O Stars and Wolf-Rayet Stars. *Astrophys. J.*, 1983, v. 274, 302–312.
7. Humphreys R. M. and Nichols M., Massey P. On the Initial Masses and Evolutionary Origins of Wolf-Rayet Stars. *Astron. J.*, 1985, v. 90, 101–108.
8. Conti P. S. and Vacca W. D. The Distribution of Massive Stars in the Galaxy: I. Wolf-Rayet Stars. *Astron. J.*, 1990, v. 100, 431–444.
9. Langer N., Hamann W.-R., Lennon M., Najarro F., Pauldrach A.Ẇ. A. and Puls J. Towards an understanding of very massive stars. A new evolutionary scenario relating O stars, LBVs [Luminous Blue Variables] and Wolf-Rayet stars. *Astron. Astrophys.*, 1994, v. 290, 819–833.
10. Crowther P. A., Smith L. J., Hillier D. J. and Schmutz W. Fundamental parameters of Wolf-Rayet stars. III. The evolutionary status of WNL [WN7 to WN9] stars. *Astron. Astrophys.*, 1995, v. 293, 427–445.
11. Hainich R., Rühling U., Todt H., Oskinova L. M., Liermann A., Gräfener G., Foellmi C., Schnurr O. and Hamann W.-R. The Wolf-Rayet stars in the Large Magellanic Cloud. A comprehendive analysis of the WN class. *Astronomy and Astrophysics*, 2014, v. 565, A27 (62 pp.).
12. Torres A. V. and Conti P. S. Spctroscopic Studies of Wolf-Rayet Stars. III. The WC Subclass. *Astrophys. J.*, 1986, v. 300, 379–395.
13. Koesterke L. and Hamann W.-R. Spectral analyses of 25 Galactic Wolf-Rayet stars of the carbon sequence. *Astron. Astrophys.*, 1995, v. 299, 503–519.
14. Barlow M. J. and Hummer D. J. The WO Wolf-Rayet stars. *Symposium – International Astronomical Union*, 1982, v. 99, 387–392.
15. Kingsburgh R. L., Barlow M. J. and Storey P. J. Properties of the WO Wolf-Rayet stars. *Astron. Astrophys.*, 1994, v. 295, 75–100.
16. van der Hucht K. A. The VIIth catalogue of galactic Wolf-Rayet stars. *New Astronomy Reviews*, 2001, v. 45, 135–232.
17. van der Hucht K. A. New Galactic Wolf-Rayet stars, and candidates (Research Note), An Annex to The VIIth Catalogue of Galactic Wolf-Rayet Stars. *Astronomy and Astrophysics*, 2006, v. 458, 453–459.
18. Galactic Wolf Rayet Catalogue. V1.25, www.pacrowther.staff.shef.ac.uk/WRcat/, Aug. 2020.
19. Mihalas D. Stellar Atmospheres, 2nd ed. W. H. Freeman and Co., San Francisco, 1978.
20. Mihalas D. and Weibel-Mihalas B. Foundations of Radiation Hydrodynamics, corr. ed. Dover Publications, New York, 1999, pp. 627–645.
21. Varshni Y. P., Talbot J., Ma Z. Peaks in Emission Lines in the Spectra of Quasars. In: Lerner E. J. and Almeida J. B., eds. 1st Crisis in Cosmology Conference, CCC-I. American Institute of Physics Conference Proceedings, v. 822, 2006.
22. Hewitt A., Burbidge G. A Revised and Updated Catalog of Quasi-stellar Objects. *Astrophys. J. Supp.*, 1993, v. 87, 451.
23. Willett C. S. Laser Lines in Atomic Species. In: Progress in Quantum Electronics, Vol. 1, Part 5, Pergamon, 1971.
24. Bennett W. R. Jr. Atomic Gas Laser Transition Data: A Critical Evaluation. IFI/Plenum, New York, NY, 1979.
25. Kramida A., Ralchenko Y., Reader J., and NIST ASD Team. NIST Atomic Spectra Database (ver. 5.8). National Institute of Standards and Technology, Gaithersburg, MD, 2020. //physics.nist.gov/asd, accessed 14 January 2021.

26. House L. L. Ionization Equilibrium of the Elements frpm H ro Fe. *Astrophys. J. Suppl.*, 1964, v. 8, 307–328.
27. Varshni Y. P. O VI and He II Emission Lines in the Spectra of Quasars. *Astrophys. Space Sci.*, 1977, v. 46, 443.
28. Maíz-Apellániz J. and Walborn N. R. A Galactic O Star Catalog. *Astrophys. J. Suppl.*, 2004, v. 151, 103–148.
29. Sota A., Maíz-Apellániz J., Walborn N. R., and Shida R. Y. The Galactic O Star Catalog V.2.0. arXiv: astro-ph/0703005.
30. Sota A., Maíz-Apellániz J., Walborn N. R., Alfaro E. J., Barrá R. H., Morrell N. I., Gamen R. C. and Arias J. L. The Galactic O-Star Spectroscopic Survey. I. Classification System and Bright Northern Stars in the Blue-Violet at R~2500. *Astrophys. J. Suppl.*, 2011, v. 193, 24–73.
31. Maíz Apellániz J., Pellerin A., Barbá R, H., Simón-Diaz S., Alfaro E. J., Morrell N. I., Sota A., Penatés Ordaz M. and Gallego Calvente A. T.. The Galactic O-Star Spectroscopic (GOSSS) and Northern Massice Dim Stars (NoMaDS) Surveys, the Galactic O-Star Catalog (GOSC), and Marxist Ghost Buster (MGB). arXiv: astro-ph/1109.1492.
32. Sota A., Maíz-Apellániz J., Morrell N. I., Barrá R. H., Walborn N. R., Gamen R. C., Arias J. L., and Alfaro E. J. The Galactic O-Star Spectroscopic Survey (GOSSS). II. Bright Southern Stars. *Astrophys. J. Suppl.*, 2014, v. 211, 10–93.
33. Maíz-Apellániz J., Moragón A. Á., de Zárate Alcarazo L. O. and the GOSSS team. The Galactic O-Star Catalog (GOSC) and the Galactic O-Star Spectroscopic Survey (GOSSS): current status. arXiv: astro-ph/1610.03320.
34. Parker Q. A., Acker A., Frew D. J., Hartley M., Peyaud A. E. J., Ochsenbein F., Phillipps S., Russell D., Beaulieu S. F., Cohen M., Köppen J., Miszalski B., Morgan D. H., Morris R. A. H., Pierce M. J. and Vaughan A. E. The Macquarie/AAO/Strasbourg Hα Planetary Nebula Catalogue: MASH. *Mon. Not. R. Astron. Soc.*, 2006, v. 373, 79–94.
35. Miszalski B., Parker Q. A., Acker A., Birkby J. L., Frew D. J. and Kovacevic A. MASH II: more planetary nebulae from the AAO/UKST Hα survey. *Mon. Not. R. Astron. Soc.*, 2008, v. 374, 525–534.
36. The Sloan Digital Sky Survey Quasar Catalog: sixteenth data release (DR16Q). www.sdss.org/dr16/algorithms/qso_catalog/, Aug. 2018.
37. scienceworld.wolfram.com/astronomy. accessed 24 Jan 2021.
38. Downes R. A., Webbink R. F., Shara M. M., Ritter H., Kolb U. and Duerbeck H. W. A Catalog and Atlas of Cataclysmic Variables: The Final Edition. *The Journal of Astronomical Data*, 2005, v. 11, 2.
39. Ramachandran V., Hamann W.-R., Oskinova L.M., Gallagher J. S., Hainich R., Shenar T., Sander A. A. C., Todt H. and Fulmer L. Testing massive star evolution, star formation history, and feedback at low metallicity. Spectroscopic analysis of OB stars in the SMC Wing. *Astronomy and Astrophysics*, 2019, v. 625, A104 (20 pp.). arXiv: astro-ph/1903.01762v2.
40. Hainich R., Pasemann D., Todt H., Shenar T., Sander A. and Hamann W.-R. Wolf-Rayet stars in the Small Magellanic Cloud. I. Analysis of the single WN stars. *Astronomy and Astrophysics*, 2015, v. 581, A21 (30 pp.).
41. Massey P. A Census of Massive Stars Across the Hertzsprung-Russell Diagram of Nearby Galaxies: What We Know and What We Don't. arXiv: astro-ph/0903.0155v2.
42. Meyer B. S., Nittler L. R., Nguyen A. N. and Messenger S. Nucleosynthesis and Chemical Evolution of Oxygen. *Review in Mineralogy & Geochemistry*, 2008, v. 68, 31–53. semanticscholar.org/paper/Nucleosynthesis-and-Chemical-Evolution-of-Oxygen-Meyer-Nittler.
43. Wallerstein G., Iben I. Jr., Parker P., Boesgaard A. M., Hale G. M., Champagne A. E., Barnes C. A., Käppeler F., Smith V. V., Hoffman R. D., Timmes F. X., Sneden C., Boyd R. N., Meyer B. S. and Lambert D. L. Synthesis of the elements in stars: forty years of progress. *Reviews of Moden Physics*, 1997, v. 69 (4), 995–1084.
44. Lengyel B. A. Introduction to Laser Physics. John Wiley, New York, 1966.
45. Willett C. S. Gas Lasers: Population Inversion Mechanisms. Pergamon Press, New York, 1974.
46. Millette P. A. Laser Action in C IV, N V, and O VI Plasmas Cooled by Adiabatic Expansion. University of Ottawa, Ottawa, ON, 1980. LaTeX typeset: researchgate.net/publication/283014713, 2015.
47. Varshni Y. P. Laser Action in Quasi-Stellar Objects? *Bull. Amer. Phys. Soc.*, 1973, v. 18, 1384.
48. Varshni Y. P. No Redshift in Quasi-Stellar Objects. *Bull. Amer. Astron. Soc.*, 1974, v. 6, 213.
49. Varshni Y. P. The Redshift Hypothesis and the Plasma Laser Star Model for Quasi-Stellar Objects. *Bull. Amer. Astron. Soc.*, 1974, v. 6, 308.
50. Varshni Y. P. Alternative Explanation for the Spectral Lines Observed in Quasars. *Astrophys. Space Sci.*, 1975, v. 37, L1.
51. Varshni Y. P. Electron Density in the Emission-Line Region of Wolf-Rayet Stars. *Astrophys. Space Sci.*, 1978, v. 56, 385.
52. Varshni Y. P. The Physics of Quasars. *Phys. Canada*, 1979, v. 35, 11.
53. Luyten W. J. A Search for Faint Blue Stars. Paper 50, University of Minnesota Observatory, Minneapolis, 1969.
54. Varshni Y. P. Proper Motions and Distances of Quasars. *Speculations in Science and Technology*, 1982, v. 5 (5), 521–532.
55. Mortlock D. J., Webster R. L. and Francis P. J. Binary Quasars. *Mon. Not. R. Astron. Soc.*, 1999, v. 309, 836–846.
56. Hennawi J. F., et al. Binary Quasars in the Sloan Digital Sky Survey: Evidence for Excess Clustering on Small Scales. *Astronomical Journal*, 2006, v. 131, 1–23.